Enhanced oxygen evolution and reduction reactions of porous ternary NiCoFe foam electrodes prepared by dynamic hydrogen template deposition

Lidija D. Rafailović*[ab], Christoph Gammer[b], Christian Rentenberger[b], Tomislav Trisović[c], Christoph Kleber[a] and H. Peter Karnthaler[b]

[a]CEST, Center of Electrochemical Surface Technology
Viktor-Kaplan- Strasse 2, 2700 Wr. Neustadt, Austria
[b]University of Vienna, Physics of Nanostructured Materials
Boltzmanngasse 5, 1090 Vienna, Austria
[c]Institute of Technical Sciences of the Serbian Academy of Sciences and Arts
Knez Mihailova 35, 11000 Belgrade, Serbia

* Corresponding author: lidija.rafailovic@cest.at

Please cite as: Nano Energy 2 (2013) 523-529
http://dx.doi.org/10.1016/j.nanoen.2012.12.004

Keywords:
Nanostructured Energy Materials
Ternary NiCoFe Electrodes
Bifunctional Catalyst
Transmission Electron Microscopy
Nanodendritic Foam Structures

Abstract

Electrodeposition at high current densities provides excellent means for the production of deposits with a high surface area. Porous deposits attract great interest due to their wide range of possible applications in electrocatalysis. In addition, an advanced porous electrode should have both, micro and nanoscaled features. We report the synthesis of a multiscale open porous foam of NiCoFe and its excellent electrocatalytic performance. At a current density of 1 A cm^{-2} a 3D dendritic structure with open pores is obtained with pore walls having a morphology that consists of 'cauliflower-like' particles containing open multiscaled dendritic structures. Cyclic voltammograms of a smooth NiCoFe electrode are compared with those of the achieved nanodendritic NiCoFe foam electrode. The catalytic activity of the NiCoFe foam is strongly enhanced for both, the cathodic reduction of oxygen and the anodic evolution of oxygen and shows a good reversibility. Therefore the presented new material is promising as bifunctional catalyst in electrochemical energy conversion and storage devices.

Introduction

Electrodeposition at high current densities provides excellent means for the production of deposits with a high surface area in the form of powders or in the form of disperse layers on the substrate [1,2]. Different processing parameters can change chemical composition, crystallite size and morphology of the deposit, which significantly alter its physical and chemical properties[1]. High surface area porous materials attract great interest due to their wide range of possible applications in electrocatalysis [3-6]. Still, the rate of electrochemical reactions is not related directly in a simple way to the surface area of the electrode since in the case of porous materials the active surface and therefore the reaction rate can be even reduced by a decrease in accessible surface area. Therefore, an advanced porous electrode should have both, micro and nanoscaled features [3]. Recently, the production of multiscale porous materials with nanoramified dendritic walls was achieved by dynamic hydrogen templating [7]. During electrodeposition of metals at high current densities hydrogen bubbles are formed in a cathodic side reaction and serve as a template for multiscale porous structures allowing the synthesis of bulk foams without introducing additional processing steps or use of hazardous chemicals. Silver [8] and gold [9] metal foam electrodes have been achieved by deposition directly on the electrode surface. Recently, we showed that CoNi dendritic alloys exhibit promising results as catalysts for oxygen evolution reaction that is of particular interest for electrochemical conversion and storage devices [10].
In this paper we report the synthesis of a multiscale open porous foam of NiCoFe and its excellent electrocatalytic performance. Oxidized FeCoNi ternary alloys have shown enhanced battery performances when used as anode in Li batteries [11]. The higher conductivity of cobalt oxy compounds in comparison to the nickel compounds lead to a better reversibility when used as positive electrode material for alkaline batteries [12]. The low thermal expansion coefficient of NiCoFe alloys allows applications as high temperature alloy [13]. It is the aim of the present work to synthesize a novel dendritic NiCoFe alloy foam electrode by dynamic hydrogen templating showing favorable features on multiple length scales: from micrometer pores to nanodendritic structures to nanograins with a high density of catalytic sites.

Experimental

The ternary alloy structures were prepared by electrodeposition on polycrystalline Ti cathodes at a constant current density of j=1 A cm^{-2} in ammonium sulfate-chloride solution (0.09M $NiSO_4$+ 0.03M $FeSO_4$+ 0.053M $CoSO_4$ + 0.4M H_3BO_3 + 0.28M NH_4Cl, at pH=2 adjusted with HCl) [14], at room temperature without stirring, using a Jaissle potentiostat, IMP 83 PC-10. For the synthesis of NiCoFe structures, Ti was used as a cathode and Ti/RuO_2, TiO_2 was used as an anode. The electrolyte solutions were made from analytical grade chemicals and high purity water. All samples were carefully treated to prevent oxidation that can be caused by their high surface area exposed to oxygen and moisture in the air [15].
The polarization measurements were carried out by a computer controlled electrochemical system (PAR M 273A) in a three-electrode compartment electrochemical cell at (298±1) K with a sweep rate of 1 mV s^{-1}. For the correction of the iR drop, a current interrupt technique was used with a time of current interruption of 0.5 s. The working electrode was a Ti rod with

a diameter of 2 mm embedded in a resin. A Pt-mesh with large surface was used as a counter electrode. The electrochemical characterization of the oxygen reduction/oxidation performance for the NiCoFe electrodes was done by linear sweep voltammetry (LSV) at a scan rate of 10 mVs^{-1} in 0.1 M KOH at pH= 12.6.
The determination of the phase content and the crystallite size was conducted by X-ray diffraction in Bragg-Brentano geometry. The evaluation was done by Rietveld refinement [16] using the TOPAS software. The morphology was analyzed with a scanning electron microscope (SEM) equipped with a field emission gun. The profile and roughness measurements were carried out from stereoscopic images using MeX software (Alicona). To analyze the foam structures in detail transmission electron microscopy (TEM) studies were carried out at 200 kV in a CM200 (Philips). TEM bright field images and diffraction patterns were recorded from pieces of the sample that were transferred to a carbon grid. To determine the crystallite size from the electron diffraction patterns, the peak analysis using selected area diffraction (PASAD) software was used [17].

Results and discussion

Figure 1 shows the results on the electrochemical behavior of NiCoFe with a polarization curve of the ternary alloy. For comparison the polarization curves of the pure metals Ni, Co and Fe were obtained with the same concentration of the respective metal ions present in the solution. It is characteristic for the iron group metals (Ni, Co and Fe) and their alloys that electrodeposition from an aqueous electrolyte is accompanied by intensive hydrogen evolution, which is caused by their negative standard electrode potentials relative to hydrogen [18]. Therefore, it is necessary to correct all polarization measurements for the iR drop in the electrolyte during the process [19,20]. The standard redox potentials of Ni^{2+}, Co^{2+}, Fe^{2+} and H^{+} are -0.52, -0.53, -0.68 and -0.24 V vs. a saturated calomel electrode (SCE), respectively. The linear sweep exhibits some similarities. As indicated in Figure 1, below - 0.6 V vs. SCE the potential shows at the beginning a region (i) of rather linear dependence on the logarithm of the current density up to a limiting current density of about $10^{-3.5}$ to $10^{-2.5}$ A cm^{-2}; this is followed by a region (ii) with almost no dependence of the potential on current density until a current density of about $10^{-0.5}$ A cm^{-2} is reached. Thereafter, in region (iii) the potential decreases strongly with increasing log j. The different regions are indicated for NiCoFe in Fig. 1. Region (i) can be explained as mixed electron transfer and diffusion control of the metal reduction reaction coinciding with limited hydrogen evolution. Region (ii) is indicative of significant hydrogen evolution. The relative overpotentials for the hydrogen evolution reaction, after iR correction, at around 0.1 A cm^{-2} at this pH, increase from Co > Fe > Ni. Region (iii) is characterized by a strong hydrogen bubble evolution and metal deposition is under diffusion control.
Figure 2 shows the structure and morphology of NiCoFe deposits obtained at different current densities. At a current density of 0.1 A cm^{-2} (sample A) a compact smooth deposit is formed (cf. Fig 2a). Only small protrusions are visible at higher magnification and the sample is completely dense (cf. insert Fig. 2a). As shown in Fig. 1 this current density represents the border between regions (ii)/(iii). Therefore mixed electron transfer and diffusion control is active leading to the formation of the smooth deposit. In contrast, at a current density of 1 A cm^{-2} (sample B) a 3D dendritic structure with open pores is obtained (Fig. 2b). The pore

walls have a finer morphology consisting of 'cauliflower-like' particles containing open multiscaled dendritic structures (as shown in the insert of Fig. 2b). The pores and microstructure are a consequence of the vigorous hydrogen gas evolution and diffusion-limited metal deposition active in region (iii) as concluded from Fig. 1. It should be noted, that the morphology of the compact smooth deposit does not change with deposition time - when deposition time is increased until the same charge is passed compared to the dendritic foam structure (t=1800 s).

The chemical composition was determined by energy dispersive X-ray spectroscopy yielding a composition of $Ni_{20}Co_{45}Fe_{35}$ in the case of the smooth deposit obtained at a current density of 0.1 A cm^{-2} (sample A). This indicates an anomalous co-deposition of the iron group elements [18] where the less noble metal is deposited preferentially to the nobler one. On the other hand in the case of the dendritic foam deposit obtained at a current density of 1 A cm^{-2} (sample B) a composition of $Ni_{50}Co_{30}Fe_{20}$, corresponding to that of the electrolyte is obtained. Intensive hydrogen evolution causes gas stirring, changing the mass transfer conditions in the double layer and hence the local electrolyte composition at the electrode surface. Under pure diffusion control the composition of the deposit is determined by the composition of the electrolyte.

Figure 2c shows the X-ray profiles corresponding to the deposits. In the case of the smooth deposit (sample A) broad peaks corresponding to the BCC structure of the (Ni,Co)Fe solid solution are shown as expected from the phase diagram for the given composition ($Ni_{20}Co_{45}Fe_{35}$) [21]. In addition the reflections arising from the Ti substrate are visible because the deposit is very thin (around 1 µm). The dendritic foam deposit (sample B) shows peaks corresponding to the FCC structure of the $(Ni,Co)_3Fe$ solid solution in accordance with the significantly different composition obtained at the higher current density ($Ni_{50}Co_{30}Fe_{20}$). No reflections from the Ti substrate are visible because the deposit is thicker (around 20 µm). In the case the smooth compact layers delimitation can occur during electrodeposition because of oxidation of Ti substrates. In contrast to that, Ti substrate represents an excellent choice for the deposition of the nanodendritic foam structure showing a uniform distribution of the deposit. The crystallite size was evaluated from the X-ray profiles by Rietveld refinement leading to an area weighted mean of 7.4 ± 1 and 6.5 ± 1 nm in the case of sample A and B, respectively. This can be correlated with the linear sweep voltammogram (cf. Fig. 1). Deposition at a current density of 0.1 A cm^{-2} belongs to region (ii) with almost no dependence of the overpotential on current. Since from the nucleation theory, the crystallite size is mainly affected by the increase of overpotential [22], the crystallite size is not changed after reaching the plateau in the polarization diagram. The increase of the overpotential with increasing current after the plateau in region (iii) is connected with an increase in hydrogen bubble evolution only.

Figure 3 shows a detailed investigation of the dendritic foam deposit by methods of electron microscopy. The 3D SEM reconstruction of surface (Fig. 3a) reveals pronounced circular depressions with about 20 µm diameter caused by the intensive gas bubble evolution. In addition a roughness on a smaller scale is encountered in the roughness profile shown as insert. Therefore to analyze the structure on an even finer length scale, a TEM investigation of the deposited FeCoNi foam was carried out. The resulting bright field image (cf. Fig. 3b) reveals dendritic branches with sizes less than 50 nm containing nanocrystals smaller than 10 nm. The corresponding TEM diffraction pattern (cf. Fig. 3c) is caused by a nanocrystalline

FCC structure. The evaluation of diffraction patterns from different areas using the PASAD software [17] leads to the result that the deposit is homogenous in structure.
Recently, we investigated the morphology of NiCoFe powders obtained by electrodeposition. TEM methods yield the results that the particles have a highly branched dendritic structure extending from the micrometer scale to the nanoscale. Since the material is deposited far off the thermal equilibrium it contains a high density of stable defects such as grain boundaries and twin boundaries, as one nanograin contains about three twins [23]. All these defects provide active sites in the form of surface steps for electrochemical reactions [24]. Therefore, the achieved dendritic NiCoFe alloy foam provides in addition to the multiscaled high surface area also a high density of active sites.
In Figure 4 cyclic voltammetry curves of both, the smooth electrode and the dendritic foam electrode are shown. The curves were recorded in a 0.1 M KOH solution at room temperature with a potential range from -400 mV to + 600 mV vs. SCE at a sweep rate of 10 mVs^{-1}. The cyclic voltammograms show reversible redox processes; oxygen reduction in the cathodic region and oxidation of NiCoFe in the anodic region. The dendritic foam electrode demonstrates a significantly enhanced reaction rate when compared with the smooth electrode. Therefore the nanodendritic NiCoFe alloy foam is a promising candidate as bifunctional catalyst in alkaline solutions. The catalytic activity is enhanced for both, the cathodic reduction of oxygen and the anodic evolution of oxygen. In the case of fuel cells, the performance of a smooth electrode is limited by the significant anodic overpotential required for oxygen evolution due to the presence of an oxide layer that covers the entire surface [25,26]. The achieved dendritic NiCoFe alloy foam on contrary shows a good reversibility and a high activity in the cathodic region. This is linked to processes involving the redox reaction between the redox couple M^{III}/M^{II}. The reversibility of the electrocatalytic processes offers the possibility to use non-noble NiCoFe transition metals for the fast electron transfer reaction between the oxidized NiCoFe dendritic alloy in dilute alkaline media that are of considerable interest for practical applications.
For the dendritic foam electrode the oxygen evolution potential is slightly positively shifted as compared to the smooth electrode and shows a significantly increased rate. Integration of the peak in the anodic region from 250 mV to 400 mV vs. SCE gives a charge of 500 mC cm^{-2} for the dendritic foam electrode. The formation of $NiCoFe_2O_4$ oxide, which is most probable at this pH, would require a charge of 0.0725 mC cm^{-2}. The enhancement in reaction rate due to the high surface area of the foam electrode can be expressed as an effective roughness factor indicating the effective surface over the geometrical area. In the present case a value of about 7000 is achieved that can be attributed to the multiscale dendritic foam structure plus taking into account in addition to the high surface area, the fact that the reaction rate is further enhanced by the presence of a high density of defects providing active sites.

Conclusion

In summary we demonstrated the excellent electrochemical features of nanodendritic NiCoFe foam. Its catalytic activity is strongly enhanced for both, the cathodic reduction of oxygen and the anodic evolution of oxygen and shows a good reversibility. Therefore it is a promising candidate as bifunctional catalyst in electrochemical conversion and storage devices. Ternary NiCoFe alloys were deposited at different current densities. At a current density of 0.1 A cm^{-2},

corresponding to mixed electron transfer and diffusion control, a smooth electrode is formed. In contrast to that during galvanostatic deposition at a high current density of 1 A cm^{-2} a multiscaled foam structure is achieved with pore sizes around 20 µm and nanodendritic walls. The dendritic branches are very fine with sizes less than 50 nm and consist of nanocrystals containing a high density of defects. The achieved dendritic NiCoFe foam electrodes show a significantly increased reaction rate for oxygen reaction when compared with the smooth NiCoFe electrode. The increase is ascribed to the multiscale 3D morphology and the defects formed during hydrogen template deposition. The resulting structure has a high surface area and a high density of active sites yielding a value of about 7000 for the effective roughness factor. In addition the composition of the achieved foam is in accordance to the chemical composition of the electrolyte, whereas the compact deposit obtained at a lower current density results in a distinct change of alloy composition content.

Acknowledgements
This research was supported by the research project "Bulk Nanostructured Materials" within the research focus "Material Science" of the University of Vienna and by the Austrian Science Fund (FWF): [S10403, P22440]. The work at CEST was supported within the COMET program by the Austrian Research Promotion Agency (FFG) and the government of Lower Austria.

[1] A Marčić, M Spasojević, L Rafailović, V Milovanović, L Ribić-Zelenović , *Mat. Sci. Forum* 453 (2004) 411.
[2] L.D. Rafailović, H.P. Karnthaler, T. Trišović, D.M. Minić, *Mat. Chem. Phys*.120 (2010) 409.
[3] S. Cherevko, C. Chung, *Electrochim. Acta* 55 (2010) 6383.
[4] A. Kloke, C. Köhler , R. Gerwig, R. Zengerle, S. Kerzenmacher, *Adv. Mater*. 24 (2012) 2916.
[5] J. Elias, M. Parlinska-Wojtan, R. Erni, C. Niederberger, F. Sauvage, M. Thevenin, J. Michler, L. Philippe, *Nano Energy* 1 (2012) 742.
[6] H.C. Shin, M.L. Liu. *Adv. Func. Mater*.15 (2005) 582.
[7] H. Shin, J. Dong, *Adv. Mater*.15 (2003) 1610.
[8] S. Cherevko, X. Xing, C. Chung, *Electrochemistry Communications*, 12 (2010) 467.
[9] S. Cherevko, C. Chung, *Electrochemistry Communications*, 13 (2011) 16.
[10] L.D.Rafailović, C. Gammer, C. Rentenberger, C. Kleber, AH. Whitehead, B. Gollas, H.P. Karnthaler, *PCCP* 14 (2012) 972-980.
[11] GF. Ortiz , J.L. Tirado, *Electrochemistry Communications* 13 (2011)1427-1430.
[12] K.H. Kim, J.Y. Zheng, W. Shin. *RSC Advances* 2 (2012) 4759-4767.
[13] X.Z. Fu, Q.C. Xu, R.Z. Hu, B.X. Pan, J.D. Lin, D.W. Liao, *Journal of power sources*, 164 (2007)916–920.
[14] Y. Sverdlov, Y. Rosenberg, Y. Rozenberg, R. Zmood, R. Erlich, S. Natan , Y. Shacham-Diamand, *Microelectronic engineering*, 76 (2004) 258.
[15] M. Pavlovic, L. Pavlovic, I. Doroslovaki, N. Nikolic, *Hydrometallurgy*, 73 (2004) 155.
[16] H. Rietveld, *Journal of Applied Crystallography* 2 (1969) 65.
[17] C. Gammer, C. Mangler, C. Rentenberger, H.P. Karnthaler, *Scripta Mater.* 63 (2010) 312.

[18] N. Zech, E. Podlaha and D. Landolt, *J. Electrochem. Soc.* 146(1999) 2886.
[19] V. Jović, B. Jović, M. Pavlović, *Electrochim. Acta* 51 (2006) 5468.
[20] L. Rafailović, D. Minić, H. Karnthaler, J.Wosik, T. Trisović, G. Nauer, *J. Electrochem. Soc.*, 157 (2010) 295.
[21] N. Nikolić, L. Pavlović, M. Pavlović, K. Popov, *Electrochim. Acta*, 52 (2007) 8096.
[22] K. Popov, S. Djokić, B. Grgur, *Fundamental aspects of electrometallurgy*, Plenum Pub Corp, 2002.
[23] L.D. Rafailović, C. Gammer, C. Kleber, C. Rentenberger, P. Angerer, H.P. Karnthaler, *Jounal of Alloys and Compounds*, 543 (2012) 167-171.
[24] I. Kasatkin, P. Kurr, B. Kniep, A. Trunschke, R. Schlögl, Angewandte Chem. 119 (2007) 7465-7468.
[25] V. Bagotsky, Fuel cells, Problems and solutions, Second edition, Wiley, 2011
[26] N. Ramaswamy, S. Mukerjee, Advances in Physical Chemistry, Article ID 491604 (2012)1-17.

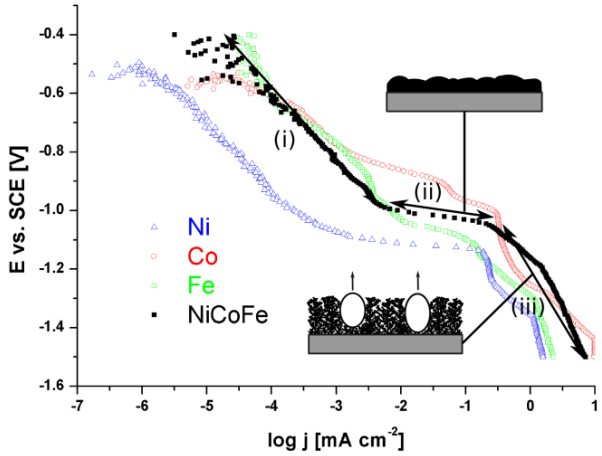

Figure 1 Linear sweep voltammograms for the electrodeposition of Ni, Co, Fe metal deposits and NiCoFe alloy deposits in ammonium sulfate-chloride solutions measured with an iR drop correction. In the case of NiCoFe, the different electrochemical regions are indicated with arrows marked (i), (ii) and (iii). Schematic representations of NiCoFe deposits obtained in region (ii) and (iii) at current densities of 0.1 and 1 A cm^{-2} respectively are shown.

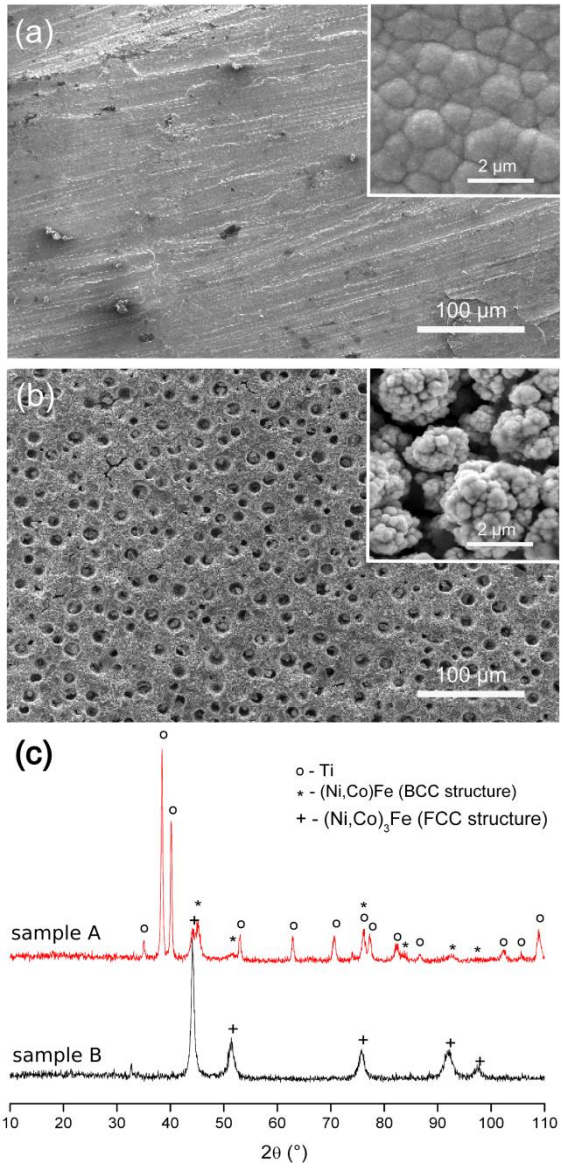

Figure 2 NiCoFe alloy deposits obtained by electrodeposition at different current densities on a Ti substrate (deposition time t=180 s): (a) SEM image of the rather smooth deposit obtained at j=0.1 A cm^{-2} characterized by a compact morphology; only at higher magnification soft hills are visible (sample A). (b) SEM image of a dendritic foam deposit obtained at j=1 A cm^{-2} showing an open porous 'cauliflower-like' morphology (sample B). (c) Corresponding X-ray profiles; the smooth deposit (sample A) shows broad peaks resulting from the nanocrystalline BCC structure of the $Ni_{20}Co_{45}Fe_{35}$ deposit and sharp peaks from to the Ti substrate; the dendritic foam deposit (sample B) shows broad peaks corresponding to the nanocrystalline FCC structure of the $Ni_{50}Co_{30}Fe_{20}$ deposit.

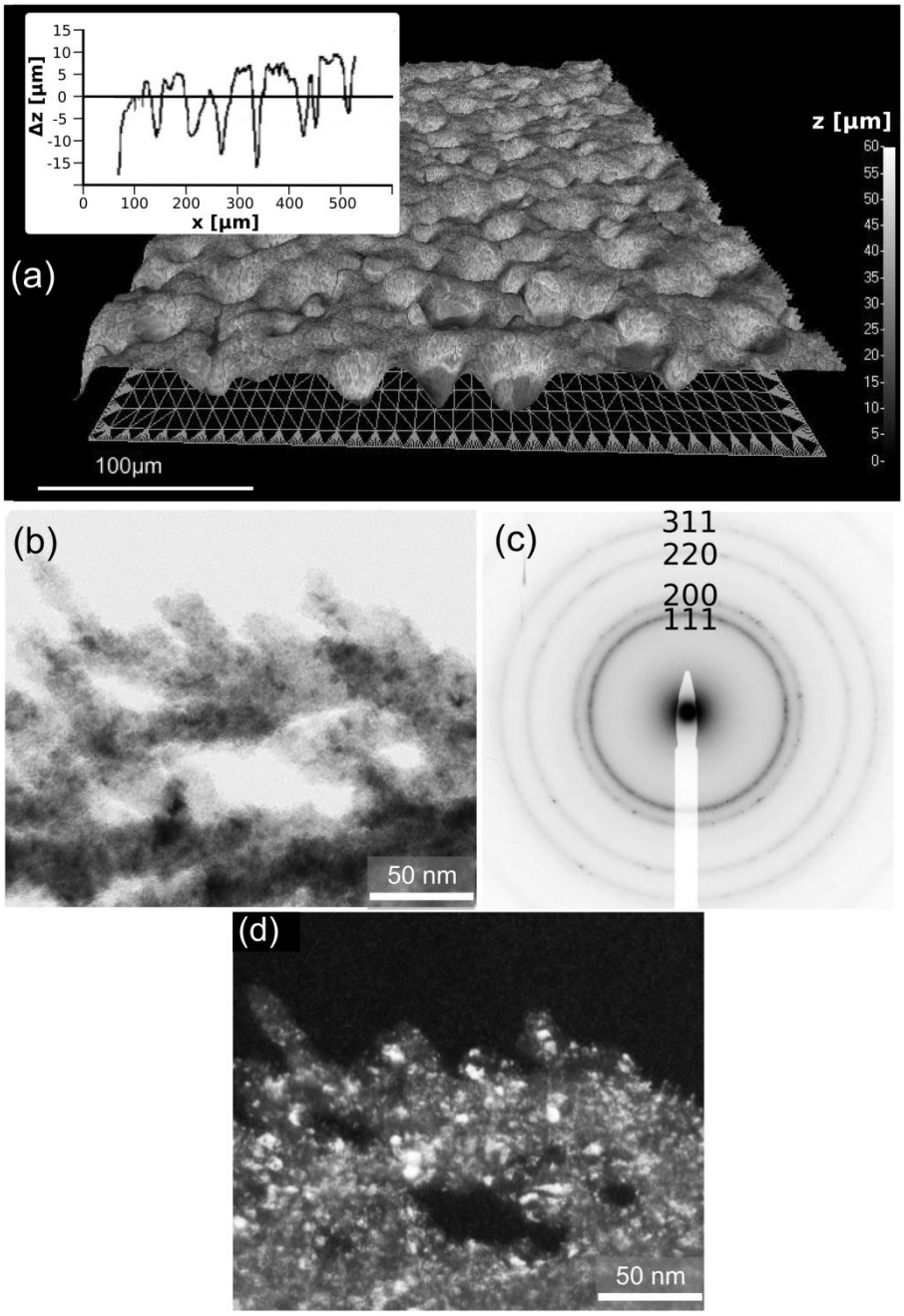

Figure 3 Open dendritic NiCoFe foam obtained by electrodeposition at a current density of j=1 A cm^{-2}. (a) 3D SEM reconstruction of the surface showing the distribution of pores formed during hydrogen co-deposition. A roughness profile across the surface is shown as insert. (b) TEM bright-field image revealing a highly branched dendritic structure. The dendrites are very fine with branches down to 50 nm. (c) The corresponding TEM diffraction pattern shows FCC structure only. (d) TEM dark-field image of the same area as (b). The dendrites consist of a nanograined structure with crystallites smaller than 10 nm.

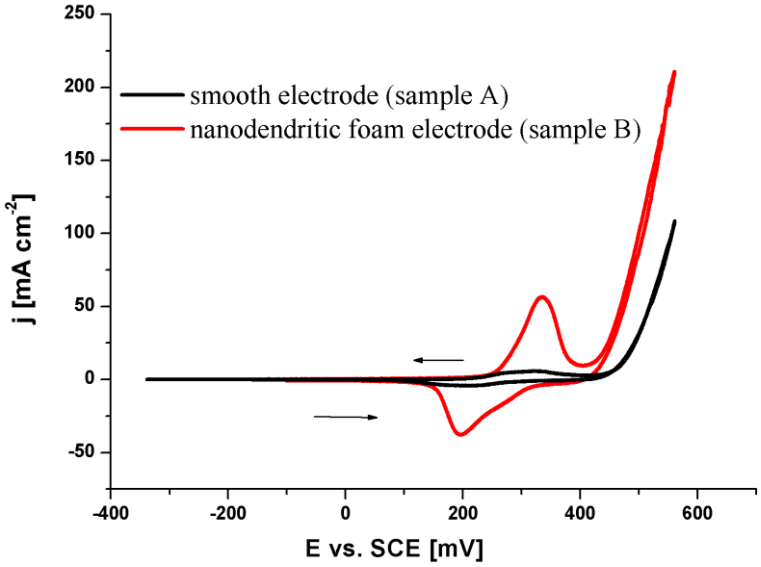

Figure 4 Cyclic voltammograms on smooth NiCoFe electrodes and dendritic NiCoFe foam electrodes recorded in 0.1M KOH solution (scan rate of 10 mV s^{-1}). The nanodendritic foam electrode shows a significantly enhanced reaction rate attributed to the multiscale dendritic foam structure.